RSC Advances

PAPER

View Article Online
View Journal | View Issue

Cite this: *RSC Adv.*, 2025, **15**, 44116

Exploring lead free Rb_2AlInX_6 halide double perovskites for advanced energy harvesting applications

Syed Muhammad Kazim Abbas Naqvi,[a] Sahar Abdalla,[b] Kiran Akhtar,[c] Aleesha Ali,[d] Nuha Y. Elamin,[b] Faheem Abbas,[e] Abdul Munam Khan[f] and Rasheed Ahmad Khera *[g]

Halide double perovskites have recently attracted attention as stable and environmentally benign alternatives to lead based perovskites for optoelectronic and energy applications. However, detailed insights into their stability, electronic structure, and multifunctional properties remain limited. In this study, the physical properties of Rb_2AlInX_6 (X = Cl, Br) were systematically examined by first-principles calculations. The structural stability of both compounds was confirmed through formation enthalpy, tolerance factor (τ_G), octahedral factor (μ), and octahedral misfit ($\Delta\mu$), all of which fall within the accepted stability ranges. Both $Rb_2AlInCl_6$ and $Rb_2AlInBr_6$ crystallize in the cubic *Fm3m* phase with optimized lattice constants of 20.37 and 21.43 bohr, respectively. Electronic structure analysis identifies both $Rb_2AlInCl_6$ and $Rb_2AlInBr_6$ as semiconducting with calculated bandgaps of 2.85 eV and 1.90 eV, respectively, underscoring their potential for optoelectronic applications. Mechanical stability, verified *via* Born criteria, was further supported by elastic tensor analysis, demonstrating isotropic and robust mechanical behavior. The $Rb_2AlInBr_6$ exhibits moderate absorption extending into the visible region, while the $Rb_2AlInCl_6$ primarily absorbs in the near UV. These features suggest potential for optoelectronic or UV photodetection applications. While thermoelectric analysis shows notable power factor values at 800 K, pointing toward possible thermoelectric applications. These findings provide a comprehensive understanding of Rb_2AlInX_6 halides, offering valuable insights into their multifunctional prospects in next generation optoelectronic and thermoelectric devices.

Received 6th September 2025
Accepted 4th November 2025

DOI: 10.1039/d5ra06712j

rsc.li/rsc-advances

Introduction

Scientists are finding novel materials that may be used to address the technical issues of the present time as technology advances, such as rechargeable battery packs that may be utilized at room temperature or above, and high stress bearing ceramics for the aviation industry.[1–3] Owing to their remarkable potential and versatility, halide double perovskites are a major topic of interest for material scientists, who have made amazing strides in developing novel materials. The formula for HDPs is $A_2BB'X_6$, where X is a halogen ion, B and B′ represent ions from magnetic or other trivalent metals, and A stands for alkali or alkaline earth compounds (or related).[4,5] Additionally, several studies have been provided to grasp the electronic, magnetic, and morphological features of HDPs. Rb_2AgAlX_6 (X = Br, I) demonstrated bandgap (E_g) of 2.60 eV and 1.08 eV, which specifies that they may absorb light energy from the UV to VIS spectrum. Their potential for incorporation into cutting-edge solar energy systems is further highlighted by the absorption band of Rb_2AgAsI_6, from 1.7 eV to 3.4 eV.[6] The direct E_g of $K_2InSbCl_6$ (1.31 eV) and $K_2InSbBr_6$ (1.22 eV) enables efficient absorption in the UV-vis regions, which makes these perfect for solar uses. Also, their excellent transport properties suggest strong potential for thermoelectric (TE) applications at 300 K.[7] Additionally, it has been effectively forecast that many stable and ecologically friendly HDPs will be viable and sustainable substitutes for solar power and thermoelectric techniques, including Rb_2YInX_6 (X = Cl, Br, I),[8] Cs_2AgInX_6 (X = F, Cl, Br, I),[9] and $Cs_2InAgCl_6$.[10] $Cs_2AgBi(Br, Cl)_6$ have indirect E_g of 2.19 and 2.77 eV, and show air stability with minimal degradation. These environmentally friendly semiconductors offer a suitable perovskite for sustainable devices.[11] Several other related HDPs

[a]*Faculty of Materials Science, Shenzhen MSU-BIT University, Shenzhen, 518115, China*
[b]*Chemistry Department, College of Science, Imam Mohammad Ibn Saud Islamic University (IMSIU), Riyadh 11623, Saudi Arabia*
[c]*Institute of Botany, University of the Punjab, Lahore 54590, Pakistan*
[d]*Chemical Engineering Research Center, School of Chemical Engineering and Technology, Tianjin University, Tianjin, China*
[e]*Department of Chemistry, Key Lab of Organic Optoelectronics and Molecular Engineering of Ministry of Education, Tsinghua University, Beijing 100084, PR China*
[f]*Department of Physics and Microelectronics, Zhengzhou University, Zhengzhou 450001, China*
[g]*Department of Chemistry, University of Agriculture, Faisalabad 38000, Pakistan. E-mail: rasheedahmadkhera@yahoo.com*

like Cs_2ErXCl_6 (X = Ag, Au).[12] $X_2ScHgCl_6$ (X = Cs, Rb)[13] and A_2YHgCl_6 (A = Cs, K)[14] were also suggested as sustainable applications.

The lack of previous research on Rb_2AlInX_6 (X = Cl, Br) offers a chance to examine their physical characteristics. This study aims to provide valuable details into the fundamental properties of both compounds and their potential applications in advanced technologies through an in-depth analysis. Such pioneering work not only expands the knowledge base of halide double perovskites but also sets the stage for their integration into future technological innovations.

Computational methods

DFT calculations were applied to investigate the electronic structure of the Rb_2AlInX_6 (X = Cl, Br).[15,16] To guarantee accurate E_g analyses, the modified Becke–Johnson (mBJ) was used, as shown by the equation below[17]

$$v_x^{mBJ} = cv_x^{mBJ}(r) - 6\frac{1}{\pi}\sqrt{\frac{5}{12}}\sqrt{\frac{2t(r)}{\rho(r)}} \quad (1)$$

It employs the electron density to determine the electronic structure. These are solved using the FP-LAPW technique.[18] The wave functions within each muffin-tin sphere are expanded using particular parameters in this technique. The R_{MT} and K_{max} products are set to 8 to guarantee accurate representation. A Monkhorst–Pack grid equivalent to 1000 k-points in the full Brillouin zone was employed to ensure accurate sampling. A convergence threshold of 0.00001 Ry for charge density was applied during self-consistent field (SCF) iterations, which ensured total energy convergence within 1×10^{-5} Ry. Energy-volume determinations were used to optimize the structure using the Murnaghan equation:[19]

$$E_{total}(v) = E_0 + \frac{B_0 V}{B_0(B_0 - 1)}\left[B_0\left(1 - \frac{V_0}{V}\right) + \left(\frac{V_0}{V}\right)^{B_0'} - 1\right] \quad (2)$$

We examined the E_g dependent optical properties using the Kramers–Kronig relations. To calculate the muffin-tin radius (R_{MT}), two conditions had to be met: (i) the MT spheres had to be free of core charge leakage, and (ii) there had to be no overlapping between the spheres. For Rb, Al, In, Cl, and Br, the R_{MT} values were 2.5, 2.15, 2.5, 2.1, and 2.38 bohr to ensure that there was no current loss. The elastic constants were computed separately using the CASTEP module in the Materials Studio package, employing a $4 \times 4 \times 4$ Monkhorst–Pack k-point grid. Additionally, TE These properties were calculated using the BoltzTraP code,[20] which employs the rigid band approximation (RBA) and the constant relaxation time approximation (CRTA). In the RBA, the effect of temperature and carrier concentration on the band structure is neglected, which may slightly affect the accuracy of Seebeck coefficient predictions at high temperatures.[21] Similarly, the CRTA assumes a constant carrier scattering time (τ) independent of temperature and energy, whereas in halide perovskites, strong electron–phonon coupling can lead to τ variations that influence both conductivity and thermopower.[22–24] These approximations, though widely used for qualitative trend analysis, may limit the precision of absolute transport coefficients. Although these approximations simplify the transport description, they remain reasonable and widely used for a first-order estimation of carrier transport.

Results and discussion

Structural features

The structural analysis reveals that Rb_2AlInX_6 (X = Cl, Br) crystallizes in a cubic structure with space group *Fm3m* (No. 225). The structure of Rb_2AlInX_6 (X = Cl, Br) is illustrated in Fig. 1 with the atomic sites of Rb, Al, In, and X at (0.75,0.25,0.25), (0,0,0), (1/2,0,0), and (0.75,0,0), correspondingly. The enhanced lattice constants for $Rb_2AlInCl_6$ and $Rb_2AlInBr_6$ are determined to be 20.37 and 21.43 bohr, correspondingly. The structures optimization is illustrated in Fig. 2 and relaxation properties are displayed in Table 1 include lattice constants (Å), optimized bulk modulus (B), its derivative (Bp), ground state energy E_0 (Ry), and volume.

A stable crystal structure is achieved by minimizing lattice strain and ensuring ideal ionic packing through a well-balanced tolerance factor. The distortion of the metal halide octahedra is also affected by octahedral misfit values, which can improve defect tolerance and adjust electronic band alignment. When constructing improved HDPs, these structural benefits are crucial since they greatly improve the material performance in optoelectronic applications.[26,27] By applying the relation given below to calculate the formation enthalpy (ΔH), the thermodynamic integrity of both HDPs is verified.

$$\Delta H = E_{Rb_2AlInX_6} - 2E_{Rb} - E_{Al} - E_{In} - 6E_X \quad (3)$$

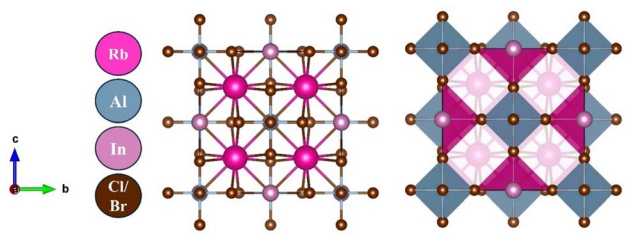

Fig. 1 Crystal structure of Rb_2AlInX_6 (X = Cl, Br).

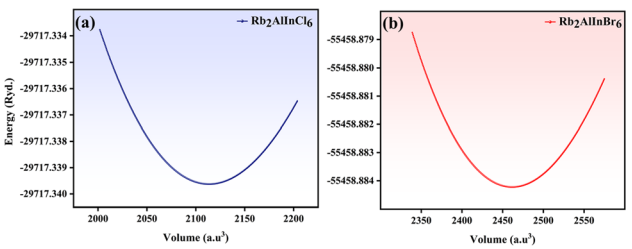

Fig. 2 Optimization in non-magnetic phase of (a) $Rb_2AlInCl_6$ and (b) $Rb_2AlInBr_6$.

Table 1 Calculated values of lattice constant (Å), B (GPa), Bp (GPa), volume (a.u),^{3} ΔH and ground state energies E_0 (Ry) of stable state of cubic Rb_2AlInX_6 (X = Cl, Br)

Parameters	$Rb_2AlInCl_6$	$Rb_2AlInBr_6$	$Rb_2InSbCl_6$ (ref. 25)	$Rb_2InSbBr_6$ (ref. 25)
Lattice constant (Å)	10.780	11.342	11.23	11.78
B (GPa)	26.170	23.7137	23.11	19.69
Bp (GPa)	5.0	5.0	4.66	4.66
V (a.u.)^3	2113.4876	2461.7013	—	—
E_0 (Ry)	−29717.339	−55458.88	—	—
τ_G	0.99	0.98	0.98	0.96
ΔH (eV)	−1.953	−3.247	−1.62	−1.34

ΔH needs to be negative to be thermodynamically stable. The calculated ΔH values for $Rb_2AlInCl_6$ are −1.953 and −3.247 eV for $Rb_2AlInBr_6$, signifying that both are robust and unlikely to degrade under typical conditions. Recent investigations on Cs_2InAsX_6 (X = Cl, Br) have shown that both are stable and exhibit negative ΔH values of −2.20 and −3.64 eV.[28] Furthermore, X_2LiSbI_6 (X = K, Cs) compounds have been reported to be dynamically stable, exhibiting negative formation energies of −3.88 eV and −3.95 eV, respectively.[29]

The stability factors like τ_G, μ, and $\Delta\mu$ are calculated to determine the stability of $Rb_2AlInCl_6$ and $Rb_2AlInBr_6$.[26,27] These are determined as:

$$\tau_G = \frac{R_{Rb} + R_X}{\sqrt{2}\left(\frac{R_{Al} + R_{In}}{2}\right) + R_X} \quad (4)$$

$$\mu = \frac{\frac{R_{Al} + R_{In}}{2}}{R_X} \quad (5)$$

$$\Delta\mu = \frac{|R_{Al} - R_{In}|}{2R_{X\,=\,Cl,\,Br}} \quad (6)$$

These are determined using ionic radii values of Rb, Al, In, and Cl/Br shown as R_{Rb}, R_{Al}, and the mean of R_{Cl} and R_{Br}. τ_G range for stable perovskites is 0.8 to 1, with unity values indicating perfect structure. The determined values of this factor are 0.99 and 0.98 for $Rb_2AlInCl_6$ and $Rb_2AlInBr_6$, confirming their stability. To confirm the validity of these results, a comparison with analogous compounds Cs_2XCeI_6 (X = Li, Na) from Murtaza *et al.*[30] showed τ values of 0.87 and 0.85 for Cs_2LiCeI_6 and Cs_2NaCeI_6. The successful synthesis of several related perovskites including $Cs_2InBiCl_6$, $Cs_2InBiBr_6$, Cs_2InBiI_6,[31] Cs_2ScAgI_6,[32] $Cs_2NaLaCl_6$,[33] Cs_2YAuBr_6,[34] $K_2InBiBr_6$,[35] and Cs_2LiCeF_6 (ref. 36) further supports their structural stability in agreement with the Goldschmidt tolerance factor model. The $\Delta\mu$ values are computed as 0.13 and 0.12 for Cl and Br perovskites, showing their stability as both are closer to the null value.[37] Moreover, the stability of these perovskites is also validated from μ values, which are calculated as 0.43 and 0.40 and exist within the standard stability range of 0.4 to 0.9 as shown in Fig. 3.[37,38]

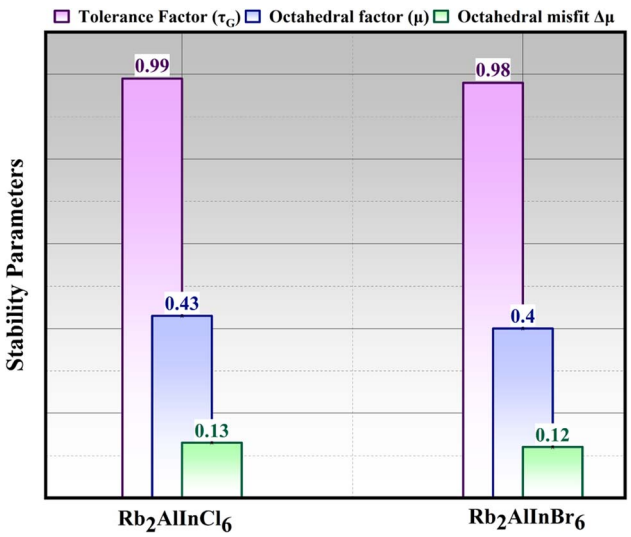

Fig. 3 Graphical representation of stability Parameters of Rb_2AlInX_6 (X = Cl, Br).

Electronic properties

To comprehend the electronic and optical characteristics $Rb_2AlInCl_6$ and $Rb_2AlInBr_6$, the electronic band structures (BS) have been examined in conjunction with their structural characteristics. By combining information about crystal structure and electronic properties, BS provides information about the conduction and basic electronic nature of halides.[39] mBJ potentials were used to calculate the BS for $Rb_2AlInCl_6$ and $Rb_2AlInBr_6$. The indirect E_g values of 2.85 eV for $Rb_2AlInCl_6$ and 1.90 eV for $Rb_2AlInBr_6$ are calculated. As the atomic radius increases from Cl to Br, this trend shows a drop in E_g, as shown in Fig. 4. To further check the relativistic effects, spin orbit coupling (SOC) was incorporated into the mBJ calculations. The inclusion of SOC slightly reduced the E_g values to 1.82 eV for $Rb_2AlInCl_6$ and 1.18 eV for E_g, without altering the indirect nature of the E_g. The overall band dispersion and density of

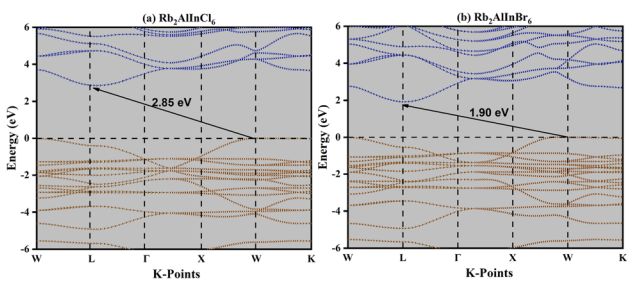

Fig. 4 Band structure of (a) $Rb_2AlInCl_6$ and (b) $Rb_2AlInBr_6$.

states (DOS) features remained qualitatively similar, confirming that SOC has only a minor influence on the electronic structure of these compounds. The corresponding SOC band structure and DOS plots are provided in the SI (Fig. S1). To assess the accuracy of our E_g calculations, we compared them with experimental E_g of well-known double perovskites. For instance, $Cs_2BiAgCl_6$ displayed a E_g of 2.2 eV, while $Cs_2AgBiBr_6$ showed a E_g of 1.95 eV.[40,41] Our predicted values are in agreement with experimental data, with small discrepancies. This comparison confirms the reliability of our E_g predictions, providing quantitative error bars for the E_g. These values are consistent with those observed in the literature and remain applicable for further exploration of related thermoelectric properties.

The total density of state (TDOS) and partial density of states (PDOS) for $Rb_2AlInCl_6$ and $Rb_2AlInBr_6$ reveal important insights into their electronic structures. In the valence band (VB) region, the In-5p orbitals show a notable contribution, indicating their strong bonding interactions with the halide atoms. For $Rb_2AlInBr_6$, the Br-4p orbitals dominate the VB and display strong hybridization with the In-5p orbitals, highlighting robust bonding. Similarly, in $Rb_2AlInCl_6$, the Cl-3p orbitals show a critical role in the VB, with prominent hybridization peaks aligning with the In-5p orbitals. Rb-5s states show negligible contribution, consistent with their non-bonding nature. Al-3p states contribute weakly near the Fermi level, indicating a minor influence on the electronic structure. In the conduction band, contributions from the In-5p orbitals dominate, along with significant involvement from Br4p in $Rb_2AlInBr_6$ and Cl-3p in $Rb_2AlInCl_6$, indicating their crucial role in optical excitation and conductivity.

The TDOS and PDOS profile of $Rb_2AlInCl_6$ and $Rb_2AlInBr_6$ is shown in Fig. 5 and 6. The changing of Br with Cl leads to a narrower valence band is observed for $Rb_2AlInCl_6$ due to the smaller ionic radius of chlorine, which strengthens bonding and pushes the valence states to slightly deeper energies, whereas the larger ionic radius of bromine in $Rb_2AlInBr_6$ leads to a broader valence band with enhanced hybridization effects. Both compounds exhibit semiconducting behaviour, with the CB dominated by In-5p and halide p-orbitals, underlining their potential for optoelectronic uses.

Optical properties

A primary consideration in determining whether solar cells are feasible for energy generation is their efficiency. The material optical characteristics, which control how it interacts with

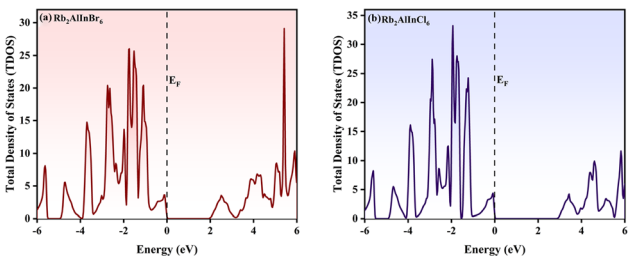

Fig. 5 Density of states (TDOS) profile of (a) $Rb_2AlInCl_6$ and (b) $Rb_2AlInBr_6$.

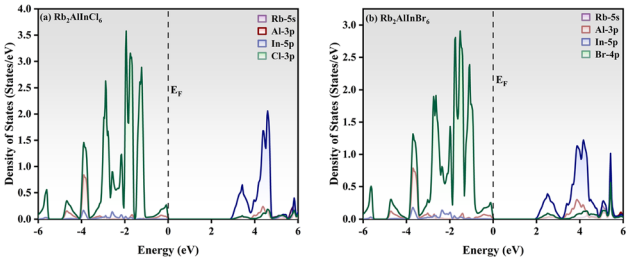

Fig. 6 Partial density of states (PDOS) profile of (a) $Rb_2AlInCl_6$ and (b) $Rb_2AlInBr_6$.

incoming electromagnetic (EM) radiation, are directly related to it.[42,43] The dielectric function $\varepsilon(\omega)$ is an intricate function that controls the relationship between a photovoltaic material and incoming EM light. It is important in this context.[44–46] The real $\varepsilon_1(\omega)$ and imaginary $\varepsilon_2(\omega)$ components of the $\varepsilon(\omega)$ can be used to obtain additional optical characteristics that further influence the material's solar power capacity. These characteristics include the absorption coefficient $\alpha(\omega)$, refractive index $n(\omega)$, reflectivity $R(\omega)$, extinction coefficient $k(\omega)$, optical conductivity $\sigma(\omega)$, and energy loss function $L(\omega)$. Scattering information is provided by $\varepsilon_1(\omega)$, while absorption attributes are provided by $\varepsilon_2(\omega)$.[47,48] The $\varepsilon_1(\omega)$ describes the degree of photon scattering and the transmission speed, which is dependent on the largest light dispersion. The static $\varepsilon_1(0)$ values for $Rb_2AlInCl_6$ and $Rb_2AlInBr_6$ are 3.15 and 3.91, respectively (Fig. 7(a)). It's interesting to note that this validation of Penn's model shows that E_g and $\varepsilon_1(0)$ have the opposite connection[49] as shown in eqn (7):

$$\varepsilon_1(0) = 1 + \left(\frac{\hbar\omega_p}{E_g}\right)^2 \quad (7)$$

A higher $\varepsilon_1(0)$ indicates a stronger interaction with the electromagnetic field and enhanced polarization under an external

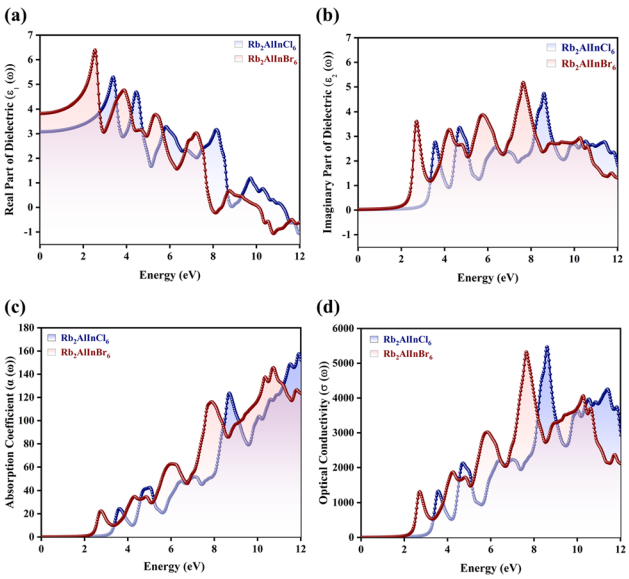

Fig. 7 Optical parameters (a) real $\varepsilon_1(\omega)$ component, (b) imaginary $\varepsilon_2(\omega)$ component, (c) absorption coefficient $\alpha(\omega)$ and (d) optical conductivity $\sigma(\omega)$ for Rb_2AlInX_6 (X = Cl, Br).

electric field, suggesting improved photon–electron coupling efficiency. For photodetectors and solar cells uses, a larger $\varepsilon_1(0)$ value is associated with increased dielectric screening and better charge separation.[50,51] Therefore, the relatively higher $\varepsilon_1(0)$ of $Rb_2AlInBr_6$ implies stronger light–matter interaction in the visible region, while the smaller $\varepsilon_1(0)$ of $Rb_2AlInCl_6$ points to faster photon transmission and suitability for UV and high frequency optoelectronic applications.

Before displaying peaks, the $\varepsilon_2(\omega)$ spectra for $Rb_2AlInCl_6$ and $Rb_2AlInBr_6$ first show a fluctuating pattern with first peaks at 3.55 eV and 2.70 eV. Some researchers calculated static $\varepsilon_1(0)$ for the similar compounds. $\varepsilon_1(0)$ values of 7.00, 3.80, 2.5, and 3.2, respectively were calculated for $Cs_2ScInBr_6$, $Cs_2ScCuCl_6$, and Cs_2ScCuF_6,[52] $Cs_2AuInCl_6$,[53] whereas Cs_2LiMoX_6 (X = Cl, I)[54] are 4.84 and 3.2037. $Na_2AuInCl_6$, $Na_2AuInBr_6$, and Na_2AuInI_6, it is calculated as 2.15, 2.34, and 3.75, respectively.[55] The $\varepsilon_2(\omega)$ component represents the optical absorption process, revealing how efficiently the material can absorb incident photons and promote interband electronic transitions. The $\varepsilon_2(\omega)$ exhibits peaks at 8.63 eV for $Rb_2AlInCl_6$ and 7.64 eV for $Rb_2AlInBr_6$, producing identical results (Fig. 7(b)). The $\varepsilon_1(\omega)$ trend across related perovskites indicates that $Cs_2InSbCl_6$ attains the highest value at 0.88 eV, with $Cs_2InSbBr_6$ and Cs_2InSbI_6 exhibiting increasing responses at 1.43 eV (5.9) and 2.87 eV (8.7), respectively, reflecting the influence of halide substitution on optical behavior.[56] The sharp peaks in $\varepsilon_2(\omega)$ confirm direct allowed transitions in both compounds, essential for visible and UV optoelectronics. However, the lower transition energy (2.70 eV) in $Rb_2AlInBr_6$ falls directly within the visible-light region, confirming its potential as a photoactive and emissive material for visible light photodetectors and LEDs.[57,58] In contrast, $Rb_2AlInCl_6$ shows its main transitions at higher energies (3.55 eV and above), suggesting it could serve effectively in UV photodetectors, transparent window layers, or protective coatings in optoelectronic devices.[59] The following equation can be used to compute it:[60]

$$\varepsilon_2(\omega) = \frac{e^2\hbar}{\pi m^2\omega^2}\sum_{vc}\int |n, n'(k,q)|^2\left[\omega n, n'(k) - \omega\right]d^3k \qquad (8)$$

The high $\alpha(\omega)$ in the visible and near UV regions[61] demonstrates strong optical activity and efficient photon utilization.[62] Such high absorption is a key requirement for photoactive absorber layers in solar cells and photodetectors, as it enables efficient electron–hole generation even in thin films.[63,64] Both $Rb_2AlInCl_6$ and $Rb_2AlInBr_6$ show considerable values throughout a wide energy range when the $\alpha(\omega)$. Both $Rb_2AlInCl_6$ and $Rb_2AlInBr_6$ exhibit significant optical transitions at 8.68 eV and 7.90 eV, respectively, in Fig. 7(c) corresponding to the deep UV region. In addition, the $Rb_2AlInBr_6$ compound shows additional weaker absorption features at lower energies, indicating a modest extension of optical activity into the visible region. This suggests that while both systems are primarily UV absorbers, the $Rb_2AlInBr_6$ possesses relatively enhanced visible light response, making it more promising for optoelectronic or photocatalytic applications. The movement of photoelectrically produced photons inside the substance is analysed by the $\sigma(\omega)$ and calculated as:

$$\sigma(\omega) = \frac{2W_{cv}\hbar\omega}{\vec{E}^2} \qquad (9)$$

The disruption of connections can be explained by the presence of strong EM radiation. $\sigma(\omega)$ exhibits free carriers produced upon capturing electromagnetic radiation, and that $\sigma(\omega)$ and $\alpha(\omega)$ are intimately associated. A maximum $\sigma(\omega)$ reflects efficient carrier transport and reduced recombination losses, both vital for high performance optoelectronic devices.[65,66] The $\sigma(\omega)$ peaks for $Rb_2AlInBr_6$ and $Rb_2AlInCl_6$ reach 5286 and 5534 Ω^{-1} cm^{-1} at 7.64 eV and 8.59 eV, respectively, indicating strong light induced carrier generation as shown in Fig. 7(d). The superior $\sigma(\omega)$ in $Rb_2AlInBr_6$ at lower photon energies suggests its carriers can be effectively excited under visible illumination, while $Rb_2AlInCl_6$, responding mainly to higher energy photons, is suitable for UV or high energy optoelectronics.[67] Together, their strong $\sigma(\omega)$ and $\alpha(\omega)$ responses confirm that both compounds can function as efficient charge transport and photon conversion layers in multi spectral optoelectronic systems.[68] While our DFT-based calculations provide a reliable estimate of the fundamental E_g, they do not account for excitonic effects, which are known to be significant in double perovskites with large exciton binding energies on the order of a few hundred m eV.[69] These effects may result in a lower optical gap compared to the DFT calculated fundamental gap.[70] However, our calculations still provide valuable insight into the material's electronic structure, and the predicted E_g remain applicable for general analysis of the material's properties. The combination of suitable E_g, high absorption, and strong conductivity indicates that $Rb_2AlInBr_6$ is more efficient for visible light optoelectronic devices such as solar absorbers, LEDs, and photodetectors, while $Rb_2AlInCl_6$, with its wider gap, can play a complementary role in UV optoelectronics and as a transparent or electron blocking layer in heterojunction structures. Further investigations incorporating excitonic effects, such as many body perturbation theory (*e.g.*, GW approximation), would enhance the accuracy of optical absorption predictions.[71,72] $k(\omega)$ is another optical characteristic that is strongly associated with $\alpha(\omega)$. The degree of damping of input photons $k(0)$ in the alloys studied is $k(\omega)$, which is brought on by both dispersion and captivation. Importantly, because they are connected by Kramers–Kronig relations, it is similar to the $\varepsilon_2(\omega)$.[73,74] The most significant values for $Rb_2AlInCl_6$and $Rb_2AlInBr_6$ emerge at 8.70 eV and 7.76 eV in the fluctuating pattern of the $k(\omega)$ spectrum (Fig. 8(a)). The overall lower extinction coefficient of $Rb_2AlInBr_6$ in the visible range minimizes optical damping and photon loss, which is beneficial for light emitting and absorbing devices, whereas the higher $k(\omega)$ in $Rb_2AlInCl_6$ contributes to its efficiency in UV photon absorption and filtering. A key indicator of the proportion of EM radiation reflecting at a particular energy is the $R(\omega)$, which is displayed in Fig. 8(b).[75,76] The $R(\omega)$ values were notable, first and foremost; for $\omega = 0$, they were 0.08 and 0.10 for $Rb_2AlInCl_6$ and $Rb_2AlInBr_6$. As energy rises, $R(\omega)$ exhibits a fluctuating trend. $R(\omega)$ is

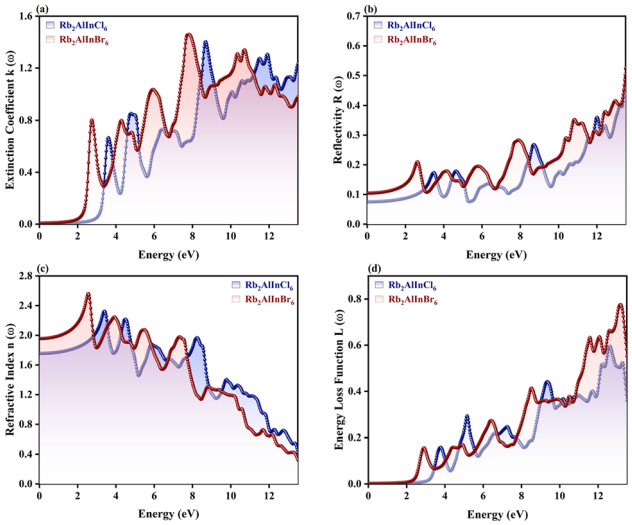

Fig. 8 Optical features of Rb_2AlInX_6 (X = Cl, Br). (a) Extinction coefficient $k(\omega)$, (b) reflectivity $R(\omega)$, (c) refractive index $n(\omega)$ and (d) energy loss function $L(\omega)$.

calculated using the provided relation, and the greatest reflectance for $Rb_2AlInCl_6$ is shown at 8.68 eV and 7.81 eV for $Rb_2AlInBr_6$. $R(\omega)$ can be computed using the relation given below:

$$R = \frac{(n-1)^2 + k^2}{(n+1)^2 + k^2} = \left|\frac{n'-1}{n'+1}\right| \quad (10)$$

Moderate reflection at low energies and increasing reflection at higher photon energies indicate balanced optical behavior for both compounds. $Rb_2AlInBr_6$, with higher reflectivity in the visible region, is promising for light emitting and laser applications, while $Rb_2AlInCl_6$, exhibiting lower reflection and higher transmission, can be applied in anti-reflective or UV transparent coatings.[77] The $n(\omega)$ varies as does $\varepsilon_1(\omega)$, an important factor for evaluating substance transparency.[78] As for $Rb_2AlInCl_6$ and $Rb_2AlInBr_6$, their respective static $n(0)$ values are 1.78 and 1.97. According to Fig. 8(c), there are other noteworthy $n(\omega)$ peaks for $Rb_2AlInCl_6$ at 3.34 eV and for $Rb_2AlInBr_6$ at 2.53 eV. The HDP analysis revealed nearly identical results. The $n(0)$ values of $Cs_2NaMoCl_6$ and $Rb_2NaMoCl_6$ were found to be 1.71 and 1.69,[79] while Rb_2YAuI_6 and Cs_2YAuI_6 demonstrated slightly higher values of 2.01 and 2.03, consistent with their heavier halide composition.[80,81] The slightly higher refractive index of $Rb_2AlInBr_6$ in the visible range ensures stronger photon confinement and efficient light–matter interaction, ideal for LEDs and photovoltaic absorbers.[82,83] Conversely, the lower $n(\omega)$ of $Rb_2AlInCl_6$ improves transparency and is suitable for UV photonics or as a top layer coating in tandem solar architectures.[84] The $L(\omega)$ shows the drop in photon energy as it passes through the material. The $L(\omega)$ peaks for $Rb_2AlInCl_6$ and $Rb_2AlInBr_6$ are seen at 9.32 eV and 8.56 eV (Fig. 8(d)). A greater $L(\omega)$ value corresponds to more pronounced plasmonic resonance and stronger collective electron oscillations. The lower energy loss of $Rb_2AlInBr_6$ indicates less internal damping and greater photon utilization in the visible region, making it favourable for LEDs and photodetectors.[85] Meanwhile, $Rb_2AlInCl_6$, with a higher $L(\omega)$ and wider E_g, is suitable for UV sensing and protective optical devices. Therefore, it can be concluded that $Rb_2AlInBr_6$, with its higher absorption coefficient, greater optical conductivity, and favourable refractive behaviour, is the most promising compound for visible light optoelectronic applications, while $Rb_2AlInCl_6$ can serve complementary roles in UV detection, high frequency photonics, and as a transparent coating layer.[86,87]

Thermoelectric features

HDPs exhibit promising TE properties because of their exceptional electronic structures, favourable carrier transport mechanisms, and tunable E_g. Their TE performance is primarily governed by a delicate balance between electrical conductivity (σ/τ), Seebeck coefficient (S), and thermal conductivity (k/τ).[88,89] Using the BoltzTraP algorithm,[20] the efficacy of $Rb_2AlInCl_6$ and $Rb_2AlInBr_6$ as TE materials is assessed. Fig. 9 presents the temperature dependent factors governing the thermoelectric performance of $Rb_2AlInCl_6$ and $Rb_2AlInBr_6$. The electronic components of k/τ are identified by the BoltzTraP code by removing the contributions from holes. A predetermined relaxation period (τ) of 10^{-14} seconds for TE characteristics is assumed in the computations. Results demonstrate a significant power factor (PF), low k/τ, and high σ/τ, which suggest strong TE efficiency. The quantity and motion of carriers are influenced by the σ/τ. Since higher T offers them the energy they need to shift, conductivity and temperature are directly correlated.[42,90] The σ/τ increases nearly linearly with temperature for both compounds, with $Rb_2AlInCl_6$ consistently higher than $Rb_2AlInBr_6$ across the entire range. At 800 K, σ/τ reaches 2.3 × 10^{19} Ω^{-1} m s^{-1} for $Rb_2AlInCl_6$ and 1.5 × 10^{19} Ω^{-1} m s^{-1} $Rb_2AlInBr_6$ as depicted in Fig. 9(a). In comparison to similar halide perovskites, this series of compounds demonstrates competitive room-temperature electric conductivity, with recorded values of 0.29 × 10^{18}, 0.21 × 10^{18}, 0.25 × 10^{18}, and 0.24 × 10^{18}

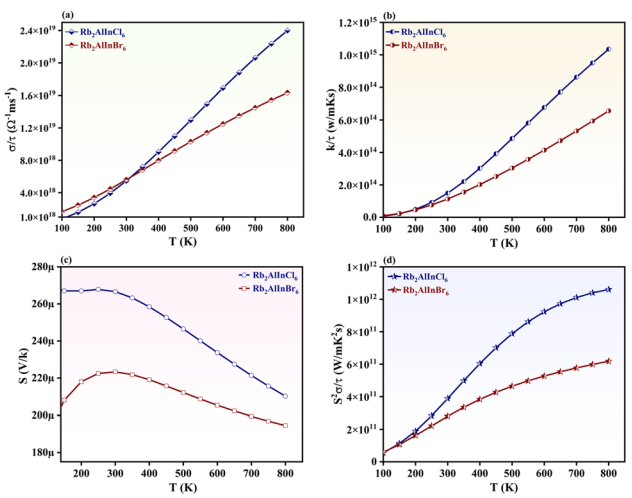

Fig. 9 Thermoelectric factors (a) electrical conductivity (σ/τ), (b) thermal conduction (k/τ) (c) Seebeck coefficient (S) and (d) power factor of Rb_2AlInX_6 (X = Cl, Br).

Ω^{-1} m s^{-1} for $K_2TlBiCl_6$, $K_2TlBiBr_6$, $Rb_2TlBiCl_6$, and $Rb_2TlBiBr_6$, respectively.[91]

The k/τ value quantifies a material's ability to conduct heat.[92,93] k/τ grows constantly with temperature. The k/τ values increase with temperature, with $Rb_2AlInCl_6$ showing higher values than $Rb_2AlInBr_6$. At 800 K, k/τ reaches 1.05×10^{15} W m^{-1} K^{-1} s^{-1} for $Rb_2AlInCl_6$ and 7.5×10^{14} W m^{-1} K^{-1} s^{-1} $Rb_2AlInBr_6$ as depicted in Fig. 9(b). Compared to similar materials, K_2AlInF_6, $K_2AlInCl_6$, and $K_2AlInBr_6$, when measured at 800 K, not only exhibit Seebeck coefficients of 150, 160, and 135 μV K^{-1}, respectively, but also a significant rise in k/τ to between 4.0–4.75 $\times 10^{14}$ W m^{-1} K^{-1} s^{-1}.[94]

S plays a key role in determining thermoelectric efficiency.[95–97] The primary carriers are holes, as shown by a positive reaction in the S spectrum.[98] This verifies the p-type nature of $Rb_2AlInCl_6$ and $Rb_2AlInBr_6$. For $Rb_2AlInCl_6$ and $Rb_2AlInBr_6$, S decreases across the whole S spectrum (Fig. 9(c)). For $Rb_2AlInCl_6$, the maximum value of S is 209 μV K^{-1} at 200 K, suggesting the TE potential of both HDPs in various uses at lower temperatures. The PF has a major effect on TE performance and can be computed as $PF = S^2\sigma/\tau$.[99] For $Rb_2AlInCl_6$ and $Rb_2AlInBr_6$, the lowest PF at 200 K is 1.35×10^{11} W K^{-2} m^{-1} s^{-1}. As the T rises, both HDP materials show a steadily growing trend in the PF plot (Fig. 9(d)). The most notable PF values for $Rb_2AlInCl_6$ and $Rb_2AlInBr_6$ at 800 K are 1.0×10^{12} W K^{-2} m^{-1} s^{-1} and 6.01×10^{11} W K^{-2} m^{-1} s^{-1}. Thermoelectric analysis of related perovskites shows that $Cs_2ScTiCl_6$ achieves a PF of 2.6×10^{-2} W m^{-1} K^{-2} s^{-1} at 800 K, closely followed by Cs_2YTiCl_6 with 2.3×10^{-2} W m^{-1} K^{-2} s^{-1}.[100] The higher PF values obtained for $Rb_2InSbCl_6$ (4.5×10^{10} W m^{-1} K^{-2} s^{-1}) and $Rb_2InSbBr_6$ (2.5×10^{10} W m^{-1} K^{-2} s^{-1}) further confirm their potential as promising thermoelectric materials.[100] The outstanding TE characteristics of $Rb_2AlInCl_6$ and $Rb_2AlInBr_6$ suggest that these compounds would be enormous options for TE generators and cooler devices.

Conclusion

In this study, the structural, electronic, optical, mechanical, and thermoelectric properties of Rb_2AlInX_6 (X = Cl, Br) halide double perovskites were comprehensively investigated using density functional theory. The electronic and optical properties were computed using the WIEN2k code with the mBJ potential for accurate estimation of E_g, while the elastic constants were calculated using the CASTEP module to validate mechanical stability. Both compounds crystallize in the stable cubic *Fm3m* phase and exhibit indirect semiconducting E_g of 2.85 eV for $Rb_2AlInCl_6$ and 1.90 eV for $Rb_2AlInBr_6$. TDOS and PDOS analyses reveal strong hybridization between In-5p and halogen-p orbitals, confirming a mixed covalent-ionic bonding nature responsible for their semiconducting behaviour. The calculated elastic constants satisfy the Born mechanical stability criteria and indicate ductile mechanical behaviour, suggesting high structural integrity under external stress. Optical analysis reveals pronounced absorption in the UV-visible region, strong dielectric response, and high optical conductivity, indicating efficient light–matter interaction suitable for optoelectronic applications. Thermoelectric calculations performed using the BoltzTraP code reveal enhanced power factors and moderate thermal conductivities, resulting in ZT values of 0.78 for $Rb_2AlInCl_6$ and 0.70 for $Rb_2AlInBr_6$ at 200 K. Collectively, the results demonstrate that $Rb_2AlInCl_6$ and $Rb_2AlInBr_6$ are mechanically and thermodynamically stable lead-free halide double perovskites, exhibiting excellent prospects for integration into high performance optoelectronic and thermoelectric energy harvesting devices.

Author contributions

S. M. K. A. Naqvi and R. A. Khera conceived and designed the study; S. Abdalla and K. Akhtar carried out the computational modelling and figure preparation; A. Ali and N. Y. Elamin contributed to data analysis and interpretation; S. M. K. A. Naqvi, F. Abbas and A. M. Khan participated in writing and editing the manuscript.

Conflicts of interest

The authors declare that they have no known competing financial interests or personal relationships that could have appeared to influence the work reported in this paper.

Data availability

All data provided and/or analysed during this study were included as figures and tables in this article.

Supplementary Information: additional results, including detailed mechanical properties and band structure/DOS graphs with spin–orbit coupling (SOC) effects. See DOI: **https://doi.org/10.1039/d5ra06712j**.

Acknowledgements

This work was supported and funded by the Deanship of Scientific Research at Imam Mohammad Ibn Saud Islamic University (IMSIU), grant number IMSIU-DDRSP2503.

References

1 Y. Zhao, A. Taheri, M. Karakus, A. Deng and L. Guo, *Minerals*, 2021, **11**, 1107.
2 X. Zhang, Y. Tang, F. Zhang and C. Lee, *Adv. Energy Mater.*, 2016, **6**(11), 1502588.
3 Q. Peng, A. Farrukh, M. Sajid, K. Shafqat, K. Muhammad, A. A. Awadh Bahajjaj, M. Nazar and J. Rehman, *J. Phys. Chem. Solids*, 2025, **196**, 112332.
4 S. Ahmad, J. Feng, M. Zakria, S. Hatim Shah, A. Alam, S. Shakeel, D. Muhammad and I. Ullah, *Mater. Sci. Eng. B*, 2024, **309**, 117641.
5 S. Choudhary, S. Tomar, D. Kumar, S. Kumar and A. S. Verma, *East Eur. J. Phys.*, 2021, **2021**, 74–80.
6 A. Mera, T. Zelai, S. A. Rouf, N. A. Kattan and Q. Mahmood, *J. Mater. Res. Technol.*, 2023, **24**, 5588–5597.
7 A. Ayyaz, G. Murtaza, A. Azazi, A. Usman, A. A. A. El-Moula, A. K. Alqorashi, F. U. R. Ahmad and M. Touqir, *Opt. Quantum Electron.*, 2024, **56**, 1204.

8 P. Aymen Nawaz, G. M. Mustafa, S. Sagar Iqbal, N. A. Noor, T. Shahzad Ahmad, A. Mahmood and R. Neffati, *Sol. Energy*, 2022, **231**, 586–592.
9 M. Tariq, M. A. Ali, A. Laref and G. Murtaza, *Solid State Commun.*, 2020, **314–315**, 113929.
10 G. Volonakis, A. A. Haghighirad, R. L. Milot, W. H. Sio, M. R. Filip, B. Wenger, M. B. Johnston, L. M. Herz, H. J. Snaith and F. Giustino, *J. Phys. Chem. Lett.*, 2017, **8**, 772–778.
11 E. T. McClure, M. R. Ball, W. Windl and P. M. Woodward, *Chem. Mater.*, 2016, **28**, 1348–1354.
12 O. Zayed, T. M. Al-Daraghmeh, Nasarullah, S. V. Menon, F. Mahmood, S. Ray, A. Sinha and A. Gautam, *J. Inorg. Organomet. Polym.*, 2025, 1–16.
13 Nasarullah, M. Nazar, S. M. K. Abbas Naqvi, G. A. A. M. Al-Hazmi and Y. M. Alawaideh, *J. Phys. Chem. Solids*, 2025, **201**, 112637.
14 K. Riaz, N. Drissi, S. Abdalla, S. Belhachi, R. Bousbih, M. S. Soliman, Nasarullah, T. H. A. Hasanin, M. Nazar and N. A. Abdulhussein, *J. Inorg. Organomet. Polym.*, 2025, **35**, 5363–5376.
15 Á. Nagy, *Phys. Rep.*, 1998, **298**, 1–79.
16 N. Argaman and G. Makov, *Am. J. Phys.*, 2000, **68**, 69–79.
17 F. Tran and P. Blaha, *Phys. Rev. Lett.*, 2009, **102**, 226401.
18 P. Blaha, K. Schwarz, P. Sorantin and S. B. Trickey, *Comput. Phys. Commun.*, 1990, **59**, 399–415.
19 F. Birch, *J. Appl. Phys.*, 1938, **9**, 279–288.
20 G. K. H. Madsen and D. J. Singh, *Comput. Phys. Commun.*, 2006, **175**, 67–71.
21 M.-S. Lee and S. D. Mahanti, *Phys. Rev. B: Condens. Matter Mater. Phys.*, 2012, **85**, 165149.
22 Y. Hattori, T. Konoike, S. Uji, Y. Tokumoto, K. Edagawa and T. Terashima, *Appl. Phys. Lett.*, 2024, **125**, 083102.
23 R. Claes, G. Brunin, M. Giantomassi, G.-M. Rignanese and G. Hautier, *Phys. Rev. B*, 2022, **106**, 094302.
24 B. Zhang, J. Klarbring, F. Ji, S. I. Simak, I. A. Abrikosov, F. Gao, G. Y. Rudko, W. M. Chen and I. A. Buyanova, *J. Phys. Chem. C*, 2023, **127**, 1908–1916.
25 D. Behera, B. Mohammed, S. Taieb, B. Mokhtar, S. Al-Qaisi and S. K. Mukherjee, *Eur. Phys. J. Plus*, 2023, **138**, 520.
26 A. E. Maughan, A. M. Ganose, M. A. Almaker, D. O. Scanlon and J. R. Neilson, *Chem. Mater.*, 2018, **30**, 3909–3919.
27 S. Ghosh, H. Shankar and P. Kar, *Mater. Adv.*, 2022, **3**, 3742–3765.
28 M. Z. Kazim, N. Raza, S. A. Aldaghfag, A. Dahshan, K. Ahmad, M. Yasar, M. Ishfaq and M. Yaseen, *J. Phys. Chem. Solids*, 2024, **189**, 111954.
29 M. Akhtar, F. K. Alanazi, M. Sajid, S. Abdalla, S. Belhachi, Nasarullah, M. Nazar, S. Murtaza, S. M. K. A. Naqvi, A. K. Alqorashi, Y. M. Alawaideh, M. Faizan and M. S. Ahmad, *J. Inorg. Organomet. Polym.*, 2025, **35**, 4810–4824.
30 H. Murtaza, Q. Ain, J. Munir, A. S. Aldwayyan, H. M. Ghaithan, A. A. Ali Ahmed and S. M. H. Qaid, *Mater. Sci. Semicond. Process.*, 2024, **181**, 108645.
31 F. Aslam, H. Ullah and M. Hassan, *Mater. Sci. Eng. B*, 2021, **274**, 115456.
32 T. Chargui, F. Lmai and K. Rahmani, *Sol. Energy*, 2024, **283**, 113016.
33 S. Shakeel, P. Song, S. H. Shah, Z. Zada, T. Huang, A. Laref, N. Hakimi and M. Faizan, *Mater. Chem. Phys.*, 2024, **324**, 129683.
34 A. Ayyaz, G. Murtaza, M. Naeem, A. Usman, S. M. Ramay, M. Irfan and H. Irfan, *J. Phys. Chem. Solids*, 2024, **188**, 111936.
35 D. Behera and S. K. Mukherjee, *JETP Lett.*, 2022, **116**, 537–546.
36 N. Rahman, A. Rauf, M. Husain, N. Sfina, V. Tirth, M. Sohail, R. Khan, A. Azzouz-Rached, G. Murtaza, A. A. Khan, S. A. Khattak and A. Khan, *RSC Adv.*, 2023, **13**, 15457–15466.
37 M. Ishfaq, M. Yaseen, S. Shukrullah and S. Noreen, *Mater. Chem. Phys.*, 2024, **313**, 128728.
38 A. El-marghany, K. Muhammad, M. Sajid, M. Nazar, M. Kashif Masood, Nasarullah, Y. M. Alawaideh and J. Rehman, *J. Phys. Chem. Solids*, 2025, **198**, 112477.
39 J. Sarkar, A. Talukdar, P. Debnath and S. Chatterjee, *J. Comput. Electron.*, 2023, **22**, 1075–1088.
40 G. Volonakis, M. R. Filip, A. A. Haghighirad, N. Sakai, B. Wenger, H. J. Snaith and F. Giustino, *J. Phys. Chem. Lett.*, 2016, **7**, 1254–1259.
41 A. H. Slavney, T. Hu, A. M. Lindenberg and H. I. Karunadasa, *J. Am. Chem. Soc.*, 2016, **138**, 2138–2141.
42 A. Ayyaz, G. Murtaza, A. Azazi, A. Usman, A. A. Abd El-Moula, A. Khadr Alqorashi, F. Ur R. Ahmad and M. Touqir, *Opt. Quantum Electron.*, 2024, **56**, 1204.
43 H. Ambreen, S. Saleem, S. A. Aldaghfag, S. Noreen, M. Zahid, Hafsa, M. Ishfaq and M. Yaseen, *Phys. B*, 2023, **667**, 415156.
44 Y. Al-Douri, M. Ameri, A. Bouhemadou and K. M. Batoo, *Phys. Status Solidi B*, 2019, **256**(11), 1900131.
45 J. Annie Abraham, D. Behera, K. Kumari, A. Srivastava, R. Sharma and S. Kumar Mukherjee, *Chem. Phys. Lett.*, 2022, **806**, 139987.
46 H. Althib, T. H. Flemban, A. I. Aljameel, A. Mera, M. G. B. Ashiq, Q. Mahmood, B. Ul Haq and S. A. Rouf, *Bull. Mater. Sci.*, 2021, **44**, 2–7.
47 M. A. Ali, M. Musa Saad H.-E., A. M. Tighezza, S. Khattak, S. Al-Qaisi and M. Faizan, *J. Inorg. Organomet. Polym. Mater.*, 2024, **34**, 1609–1619.
48 K. Assiouan, A. Marjaoui, J. EL Khamkhami, M. Zanouni, H. Ziani, A. Bouchrit and A. Achahbar, *J. Phys. Chem. Solids*, 2024, **188**, 111890.
49 D. Penn, *Phys. Rev.*, 1962, **128**, 2093.
50 R. Su, Z. Xu, J. Wu, D. Luo, Q. Hu, W. Yang, X. Yang, R. Zhang, H. Yu, T. P. Russell, Q. Gong, W. Zhang and R. Zhu, *Nat. Commun.*, 2021, **12**, 2479.
51 B. Bernardo, D. Cheyns, B. Verreet, R. D. Schaller, B. P. Rand and N. C. Giebink, *Nat. Commun.*, 2014, **5**, 3245.
52 G. Ayub, N. Rahman, M. Husain, M. Sohail, R. Khan, N. Sfina, M. Elhadi, A. Azzouz-Rached and A. Alotaibi, *J. Phys. Chem. Solids*, 2024, **188**, 111942.
53 S. Mahmud, M. A. U. Z. Atik, M. N. Mostakim, Md. Tarekuzzaman and Md. Z. Hasan, *Comput. Condens. Matter*, 2024, **40**, e00950.

54 Nasarullah, R. Bousbih, M. Sajid, T. Sattar, A. S. Alshomrany, S. Alharthi, M. A. Amin, Y. A. El-Badry, M. Shaban, A. Ahmad and M. Nazar, *Phys. B*, 2024, **687**, 416070.
55 H. D. Alkhaldi, *J. Inorg. Organomet. Polym.*, 2025, **35**, 3260–3274.
56 S. Tariq, L. El Hachemi Omari, V. Tuyikeze and M. Abid, *Mater. Today: Proc.*, 2023, DOI: 10.1016/j.matpr.2023.11.149.
57 I. E. Castelli, K. S. Thygesen and K. W. Jacobsen, *J. Mater. Chem. A*, 2015, **3**, 12343–12349.
58 M. Shirayama, H. Kadowaki, T. Miyadera, T. Sugita, M. Tamakoshi, M. Kato, T. Fujiseki, D. Murata, S. Hara, T. N. Murakami, S. Fujimoto, M. Chikamatsu and H. Fujiwara, *Phys. Rev. Appl.*, 2016, **5**, 014012.
59 W. Meng, X. Wang, Z. Xiao, J. Wang, D. Mitzi and Y. Yan, *J. Phys. Chem. Lett.*, 2017, **8**, 2999–3007.
60 M. Asghar, H. S. Waheed, U. Abbas, H. Ullah, M. J. I. Khan, S. M. Wabaidur, A. Ali and Y.-H. Shin, *Phys. B*, 2024, **682**, 415916.
61 S. A. Khandy, I. Islam, K. Kaur, A. M. Ali and A. F. A. El-Rehim, *Mater. Chem. Phys.*, 2023, **297**, 127293.
62 M. Y. H. Khan, S. S. Hasan, Md. Z. Rahman, Md. Rasheduzzaman and Md. Z. Hasan, *RSC Adv.*, 2025, **15**, 34643–34668.
63 H. Kim, H. Kwak, I. Jung, M. S. Kim, J. Kim, H. J. Park and K.-T. Lee, *Opt. Express*, 2021, **29**, 35366.
64 F.-T. Zahra, M. M. Hasan, Md. B. Hossen and Md. R. Islam, *Heliyon*, 2024, **10**, e33096.
65 N. Algethami, A. Jehan, N. Rahman, S. Naz Khan, W. Mohammed Almalki, M. Husain, V. Tirth, H. A. Althobaiti, Y. M. Alawaideh, K. M. Abualnaja and G. Alosaimi, *Results Phys.*, 2025, **70**, 108163.
66 S. Nabi, A. W. Anwar, Z. Wazir, S. S. Hayat, M. Ahmad, M. Tayyab, K. Nabi, M. Shamoil, A. A. Khan and B. S. Khan, *Eur. Phys. J. B*, 2022, **95**, 55.
67 A. Shukla, V. K. Sharma, S. K. Gupta and A. S. Verma, *Mater. Res. Express*, 2020, **6**, 126323.
68 R.-I. Biega, M. R. Filip, L. Leppert and J. B. Neaton, *J. Phys. Chem. Lett.*, 2021, **12**, 2057–2063.
69 F. Zhang, W. Gao, G. J. Cruz, Y. Sun, P. Zhang and J. Zhao, *Phys. Rev. B*, 2023, **107**, 235119.
70 F. M. Dezashibi, A. Doroudi and H. Noshad, *Optik*, 2023, **295**, 171475.
71 F. Sagredo, S. E. Gant, G. Ohad, J. B. Haber, M. R. Filip, L. Kronik and J. B. Neaton, *Phys. Rev. Materials*, 2024, **8**, 105401.
72 V. B. Bobrov, S. A. Trigger, G. J. F. van Heijst and P. P. J. M. Schram, *Europhys. Lett.*, 2010, **90**, 10003.
73 I. Moreels, G. Allan, B. De Geyter, L. Wirtz, C. Delerue and Z. Hens, *Phys. Rev. B: Condens. Matter Mater. Phys.*, 2010, **81**, 235319.
74 W. Jiang and X. Chen, *AIP Adv.*, 2022, **12**, 065106.
75 A. Bibi, I. Lee, Y. Nah, O. Allam, H. Kim, L. N. Quan, J. Tang, A. Walsh, S. S. Jang, E. H. Sargent and D. H. Kim, *Mater. Today*, 2021, **49**, 123–144.
76 K. V. Baryshnikova, M. I. Petrov, V. E. Babicheva and P. A. Belov, *Sci. Rep.*, 2016, **6**, 22136.
77 Nasarullah, M. Z. Choudary, S. A. Aldaghfag, Misbah, M. Yaseen, M. Nazar and R. Neffati, *Phys. Scr.*, 2022, **97**, 105705.
78 A. El-marghany, K. Muhammad, M. Sajid, M. Nazar, M. K. Masood, Nasarullah, Y. M. Alawaideh and J. Rehman, *J. Phys. Chem. Solids*, 2025, **198**, 112477.
79 A. Khan, M. Saeed, A. R. Chaudhry, M. A. Jehangir, M. Ibrar and G. Murtaza, *Solid State Commun.*, 2024, **394**, 115698.
80 A. Nazir, A. Dixit, E. A. Khera, M. Manzoor, R. Sharma and A. J. A. Moayad, *Mater. Adv.*, 2024, **5**, 4262–4275.
81 T. D. Flaim, Y. Wang and R. Mercado, *Advances in Optical Thin Films*, 2004, vol. 423.
82 J. B. Khurgin, *ACS Photonics*, 2022, **9**, 743–751.
83 J.-M. Renoirt, C. Zhang, M. Debliquy, M.-G. Olivier, P. Mégret and C. Caucheteur, *Opt. Express*, 2013, **21**, 29073.
84 S. V. Boriskina, T. A. Cooper, L. Zeng, G. Ni, J. K. Tong, Y. Tsurimaki, Y. Huang, L. Meroueh, G. Mahan and G. Chen, *Adv. Opt. Photon*, 2017, **9**, 775.
85 D.-Y. Li, H.-Y. Kang, Y.-H. Liu, J. Zhang, C.-Y. Yue, D. Yan and X.-W. Lei, *Chem. Sci.*, 2024, **15**, 953–963.
86 B. Zhou and D. Yan, *Matter*, 2024, **7**, 1950–1976.
87 F. Aslam, B. Sabir and M. Hassan, *Appl. Phys. A:Mater. Sci. Process.*, 2021, **127**, 1–12.
88 H. A. Alburaih, *J. Alloys Compd.*, 2021, **876**, 159806.
89 S. A. Aldaghfag, A. Aziz, A. Younas, M. Yaseen, A. Murtaza and H. H. Hegazy, *J. Solid State Chem.*, 2022, **312**, 123179.
90 K. Rangar, A. Soni and J. Sahariya, *Multiscale and Multidiscip. Model. Exp. and Des.*, 2025, **8**, 451.
91 A. Gilani, Nasarullah, S. A. Aldaghfag and M. Yaseen, *J. Phys. Chem. Solids*, 2023, **175**, 111208.
92 K. A. Alrashidi, A. Dixit, A. Nazir, E. A. Khera, S. Mohammad, M. Manzoor, R. Khan and R. Sharma, *J. Inorg. Organomet. Polym.*, 2025, **35**, 1764–1778.
93 S. Saidi, S. Belhachi, S. Abdalla, J. Y. Al-Humaidi, M. W. Iqbal, M. S. M. Al-Saleem, M. M. Rahman, M. Sillanpää, A. Kumar and S. Singh, *J. Comput. Chem.*, 2025, **46**, e70222.
94 E. Haque and M. A. Hossain, *J. Alloys Compd.*, 2018, **748**, 63–72.
95 Y. Wang, Y.-J. Hu, B. Bocklund, S.-L. Shang, B.-C. Zhou, Z.-K. Liu and L.-Q. Chen, *Phys. Rev. B*, 2018, **98**, 224101.
96 J. Martin, L. Wang, L. Chen and G. S. Nolas, *Phys. Rev. B:Condens. Matter Mater. Phys.*, 2009, **79**, 115311.
97 J. De Boor and E. Müller, *Rev. Sci. Instrum.*, 2013, **6**, 84.
98 T. S. Ahmad, N. Ehsan, M. Liaqat, S. M. S. Gilani, A. ul Haq, A. M. Quraishi, D. Abduvalieva, V. Tirth, A. Algahtani, R. M. Mohammed, N. M. A. Hadia, A. Mohammed Alsuhaibani, M. S. Refat and A. Zaman, *Results Phys.*, 2024, **63**, 107885.
99 S. A. Aldaghfag, S. Saleem, Nasarullah, M. Arshad and M. Yaseen, *Phys. B*, 2024, **677**, 415700.
100 D. Behera, B. Mohammed, S. Taieb, B. Mokhtar, S. Al-Qaisi and S. K. Mukherjee, *Eur. Phys. J. Plus*, 2023, **138**, 520.